4D microstructural changes in dentinal tubules during acid demineralisation

Leung, Nathanael; Harper, Robert; Shelton, Richard; Landini, Gabriel; Sui, Tan

DOI:
10.1016/j.dental.2021.09.002

4D microstructural changes in dentinal tubules during acid demineralisation

Nathanael Leung[a], Robert A. Harper[b], Bin Zhu[a], Richard M. Shelton[b], Gabriel Landini[b], Tan Sui[a*]

[a] Bioinspired Materials Group, Department of Mechanical Engineering Sciences, University of Surrey, Guildford, Surrey, GU2 7XH, U.K.

[b] School of Dentistry, College of Medical and Dental Sciences, University of Birmingham, 5 Mill Pool Way, Edgbaston, Birmingham, B5 7EG, U.K.

* Corresponding author: t.sui@surrey.ac.uk

Abstract

Objective

Dental erosion is a common oral condition caused by chronic exposure to acids from intrinsic/extrinsic sources. Repeated acid exposure can lead to the irreversible loss of dental hard tissues (enamel, dentine, cementum). Dentine can become exposed to acid following severe enamel erosion, crown fracture, or gingival recession. Causing hypersensitivity, poor aesthetics, and potential pulp involvement. Improving treatments that can restore the structural integrity and aesthetics are therefore highly desirable. Such developments require a good understanding of how acid demineralisation progresses where relatively little is known in terms of intertubular dentine (ITD) and peritubular dentine (PTD) microstructure. To obtain further insight, this study proposes a new in vitro method for performing demineralisation studies of dentine.

Methods

Advanced high-speed synchrotron X-ray microtomography (SXM), with high spatial (0.325 μm) and temporal (15 min) resolution, was used to conduct the first in vitro, time-resolved 3D (4D) study of the microstructural changes in the ITD and PTD phases of human dentine samples (~0.8×0.8×5 mm) during 6 h of continuous acid exposure.

Results

Different demineralisation rates of ITD (1.79 µm/min) and PTD (1.94 µm/min) and their progressive width-depth profiles were quantified, which provide insight for understanding the mechanisms of dentine demineralisation.

Significance

Insights obtained from morphological characterisations and the demineralisation process of ITD and PTD during acid demineralisation would help understand the demineralisation process and potentially aid in developing new therapeutic dentine treatments. This method enables continuous examination of relatively large volumes of dentine during demineralisation and also demonstrates the potential for studying the remineralisation process of proposed therapeutic dentine treatments.

Keywords: Acid demineralisation; Synchrotron X-ray microtomography (SXM); Time-resolved 3D analysis; Erosion; Peritubular dentine (PTD); Intertubular dentine (ITD)

Graphical Abstract

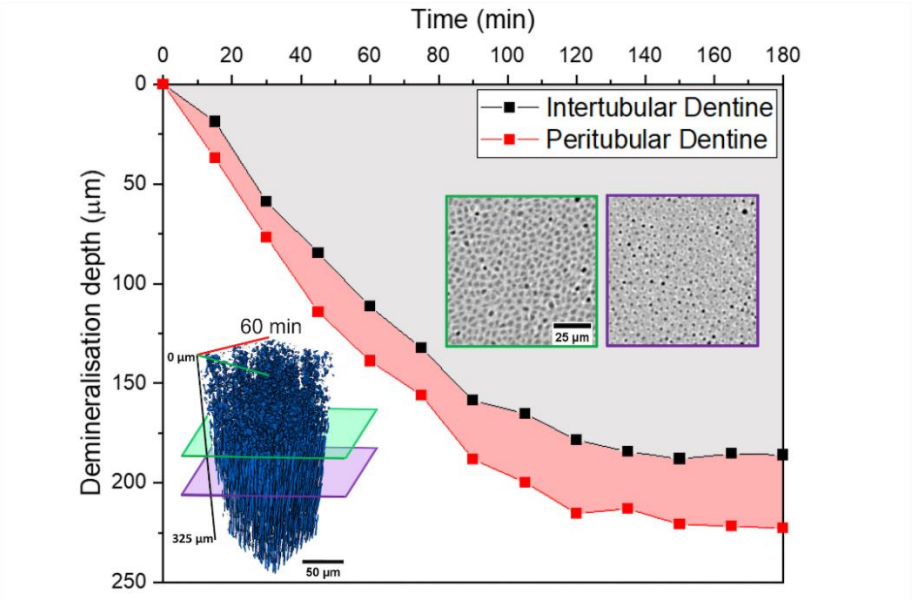

Highlights

- *In situ* high-speed synchrotron X-ray tomography study of dentine demineralisation.
- Submicron-scale dimensional changes measured at ~15-min time intervals.
- Tubule dimensions measured to a depth of 325 µm

1. Introduction

Dental erosion is the irreversible loss of dental hard tissues due to chemical dissolution by acids of non-bacterial origin [1]. The source of acid can be intrinsic (gastric acid, i.e. hydrochloric acid) [2], or extrinsic (dietary acids, medication or the environment) [3]. For the general populace, the primary source of acids are from acidic foods and beverages containing various acids including acetic, citric, lactic, malic and tartaric [4]. The inorganic composition of mineralised dental tissues mostly consists of a substituted form of hydroxyapatite (HAp), described as a calcium-deficient carbonated HAp with some fluoride [5]. In the oral environment, HAp in the dental tissues is in ionic homeostasis between demineralisation and remineralisation, represented by the simplified chemical equation:

$$Ca_{10}(PO_4)_6(OH)_2 + 8H^+ \rightleftharpoons 10Ca^{2+} + 6{HPO_4}^{2-} + 2H_2O \quad (1)$$

where demineralisation is the reaction going from left to right [6]. This homeostasis is maintained by hydroxycarbonate and phosphate buffers and inorganic Ca^{2+} and F^- ions from saliva. When exposed to acids, the low pH disrupts the ionic balance and results in the loss of minerals in the teeth. In response, salivary flow is increased to deliver more buffers and ions that neutralise the acid and allow for remineralisation to occur. However, this remineralisation is limited and ultimately results in net mineral loss depending on the severity of the acid exposure [7].

Dentine forms the main bulk of the tooth, supporting enamel that encapsulates the crown and cementum as the superficial layer on the root of the tooth. At the microscopic scale, dentine is structurally anisotropic with numerous tubules containing odontoblast processes [8]. In between these tubules there is *intertubular dentine* (ITD), composed of plate-like HAp crystallites (3 nm thick, 60 nm long) embedded in a dense matrix of collagen fibrils. Around the lumen of the tubules, *peritubular dentine* (PTD) appears more mineralised than ITD and consists of isodiametric HAp crystallites, (~25 nm in diameter) embedded in a non-collagenous matrix of phospholipids and proteins [9]. Although it is generally inaccessible to the oral environment, dentine can become exposed to acids in the mouth after enamel or cementum have been lost due to dental attrition,

abrasion, erosion, or following dental fracture. Despite having a higher degree of mineralisation, the finer-sized HAp crystallites provides a higher surface-to-volume ratio that makes PTD more susceptible than ITD to acid dissolution [10]. As such, the demineralisation process starts in PTD, causing dentinal tubules to widen and eventually affects ITD, leaving a superficial layer of demineralised collagen [11] which can be broken down by bacteria and host enzymes, such as matrix metalloproteinases [12].

Past observational studies of dentinal tubules at the micro- and nanoscales with conventional and advanced microscopy techniques such as scanning electron (SEM), [13], transmission electron (TEM) [14] and atomic force microscopy (AFM) [15] have allowed observation of the microstructure and mechanical properties of PTD and ITD after *ex situ* acid demineralisation. Those techniques revealed important characteristic changes in PTD and ITD, although *ex situ* experiments captured information from the end-result, not during the process of demineralisation and lacked the detail of time-resolved analysis. In addition, TEM requires destructive preparations of the samples which means that is it impossible to make time-resolved observations of the same tubules during demineralisation and SEM does not allow real time *in situ* experimentation. More insightful observations could be made from 3D studies of the dentinal structure collected in a time-resolved manner (simply referred to as 4D studies). which have been performed using AFM [16–20]. However, observations were limited to a depth of ~2 μm from the sample surface as PTD quickly demineralises beyond the reach of the AFM probe which then is unable to examine the mineralised ITD beyond the demineralised collagen matrix at the sample surface. Hence, that technique is only capable of characterising the initial stages of dentine demineralisation. X-ray micro-computed tomography (XMT) is non-destructive and enables observation of large 3D volumes, allowing the progression of demineralisation to be monitored at depths that are hundreds of micrometres beyond the capabilities of AFM. XMT has been used to visualise dentinal tubules with submicron resolution and reasonable contrast between ITD and PTD [21–24]. XMT was also used to study interrupted *ex situ* dentine demineralisation (where a sample was demineralised for a period outside the instrument

before scanning and following this was taken out and demineralised further and the process repeated.) [14,25] to measure and map mineral densities although without sufficient spatial resolution to observe structural changes of dentinal tubules. Therefore, it has not been possible to make complete observations of the 3D spatio-temporal changes occurring in ITD and PTD during demineralisation which are essential for understanding the processes involved.

High-speed synchrotron X-ray microtomography (SXM) is capable of high spatial and temporal resolutions, compared with other X-ray techniques and is ideally suited for time-resolved studies. The authors therefore propose this technique as a method for 4D dentine demineralisation studies. The present study aims to identify demineralisation rates, structural and dimensional changes, by means of time-resolved, submicron resolution SXM to determine its suitability for such studies. To the authors' best knowledge, this is the first investigation of continuous PTD and ITD demineralisation using high-speed SXM to reveal 3D microstructural dentine changes with time.

2. Materials and Methods

2.1 Sample Preparation

Non-carious human third molars, extracted at the Birmingham Dental School and Hospital for therapeutic reasons (BCHCDent332.1531.TB, REC Ref.:14/EM/1128), were fixed in 10% neutral buffered formalin (Sigma Aldrich, UK). Samples (~0.8×0.8×5 mm dentine cuboids) were prepared using a low-speed diamond bone saw (Isomet™, Buehler, UK) by first cutting a ~1 mm thick section ±0.5 mm either side of the centre of the occlusal surface, cutting from the crown to the root. A further two cuts were made to generate a cuboid of dentine/enamel (from the mid occlusal surface) and a final cut around the dentinoenamel junction to isolate the dentine. The cuboids were ground to a width and depth of 0.8 mm, with 0.02 mm tolerance. To ensure a tolerance of 0.02 mm, the samples were radiographed to measure dimensions and polished with a whetstone to make fine adjustments, if required. Finally, the pulpal side of the dentine samples was polished using diamond paste (DP-Paste P, 0.25 μm, Struers Ltd, UK) on a Texmet® polishing cloth (Buehler, UK). After polishing, the

samples were rinsed in deionised (DI) water to remove particulates and then imaged using light microscopy to check that there were no diamond particles remaining in the sample. To prevent unwanted acid exposure, five sides of the dentine cuboids were coated with nail varnish (Color Club®), leaving the top surface (pulpal dentine side) exposed. After preparation, each sample was immersed in phosphate buffered saline solution (~1 mL, Sigma Aldrich, UK) at pH 7.4 at 4 °C. To test whether SXM was a suitable method for time-resolved investigations of dentine demineralisation, this method of preparation was chosen with the primary focus of producing samples that were as uniform as possible.

2.2. *In situ* Synchrotron X-ray Microtomography (SXM) Setup

2.2.1. Dentine Demineralisation Setup

Kapton® polyimide sheets (DuPont™, USA) were rolled into tubes of approximately the same width as the sample and 15 mm height held together with cyanoacrylate (Loctite®). The sample was then inserted into the base of the tube, with the exposed surface facing upwards, before being fixed in place with nail varnish as an adhesive. The remaining length of the tube acted as a reservoir to contain the acid solution. The setup is shown in Figure 1b and three samples were tested.

An aqueous solution of 10% v/v lactic acid (pH 2, 100 µL) was used in the present study to simulate the acid demineralisation of dentine within a reasonable timescale [26], for the synchrotron experiment. The lactic acid solution (Hopkin & Williams Ltd, UK) was 88% v/v and was diluted with DI water to the desired concentration. During erosion and caries, the amount of acid is limited and undergoes cycles of pH changes. To replicate a single pH cycle, a finite quantity of acid solution was added to the Kapton tube using a syringe (3 µL of the solution) and the top of the tube was sealed with dental ribbon-wax (Metrodent, UK) to prevent evaporation.

2.2.2. X-ray Microtomography Setup

The experiment was conducted using absorption contrast imaging on the Diamond Manchester Branchline I13-2 at Diamond Light Source (DLS, UK). Fast acquisition times were achieved by using a polychromatic pink beam (17.5 keV) as the high intensity reduced the exposure time of each *in situ* tomographic projection (a trade-off between accurately measuring mineral density and scanning speed). Tomographic data was collected using a pco.edge 5.5 detector (PCO AG, Germany, 10× magnification, effective pixel size: 0.325 µm, field of view: 0.83×0.7 mm) (Figure 1a) with a propagation distance of 70 mm. Each tomographic scan consisted of 3001 projections (individual radiographs) collected at equally spaced angles over 180^{o} of continuous rotation ("fly-scan") with an exposure time of 300 ms, achieving the fastest possible scan time of 15 min. A scan of the sample without acid provided a reference which was then followed by the addition of acid. Scans were then carried out back-to-back for a total of 6 h.

2.3. Tomographic Reconstruction and Analysis

2.3.1. 3D Data Processing

Tomographic projection images were flat- and dark-field corrected before reconstruction into 3D volumes using a filtered back projection algorithm, performed using the visualisation and analysis software DAWN [27,28]. This produced a stack of 2160 images (32-bit greyscale, 2560×2560 pixels), that were converted to 8-bit and cropped to a volume of interest (VOI), with a cross-section of 300×300 pixels (97.5×97.5 µm^2). The VOIs were taken from the region close to the sample centre where there were less tomography artefacts. This VOI was then kept the same for each timepoint of the respective sample. For quantitative analysis, 3D datasets were reduced to a height of 1000 pixels (325 µm) to reduce the necessary computation time, with the top slice located just above the sample surface. For 3D visualisation with Avizo software (FEI Visualization Sciences Group, France), datasets were reduced in height, to only include the ITD demineralisation, starting from the same top slice. Following reconstruction, images were further processed using ImageJ (Fiji distribution)

platform [29,30]. To reduce noise whilst minimising the blurring effect, the images were filtered using a 3D median filter with a 3×3×3 kernel. To analyse the tubules, images were binarised by global thresholding with the *Auto Threshold* tool in ImageJ, using Otsu's thresholding algorithm on the stack histogram [31]. An example of this thresholding is shown in Figure 1c and d.

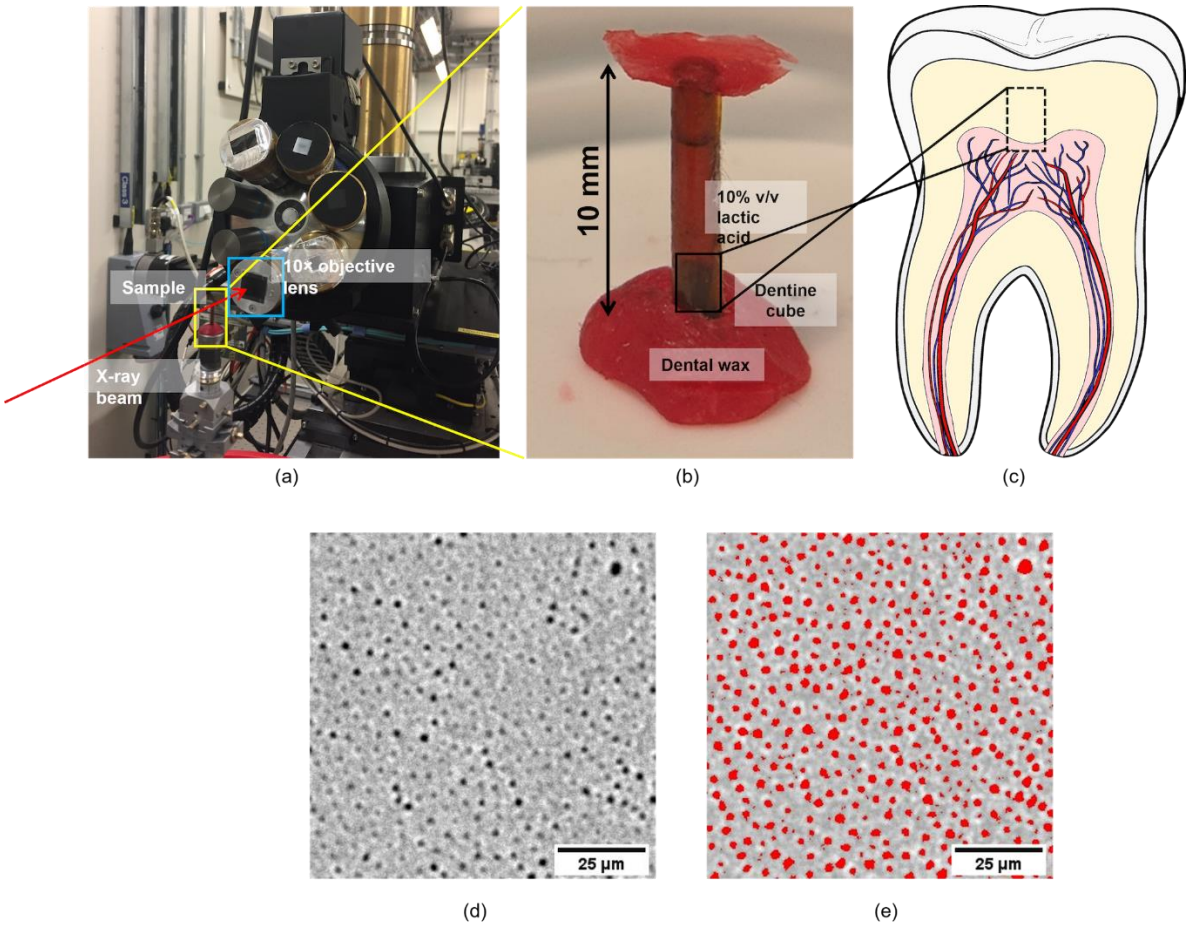

Figure 1 Microtomography experimental set-up and image processing steps. (a) The direction of the X-ray beam is indicated by the red arrow. Yellow rectangle highlights the sample position. Samples were scanned using a 10× objective lens, highlighted by the blue rectangle. (b) Image of the sample setup. A varnished dentine cuboid was encased at the bottom of a Kapton scroll, with an exposed surface facing up. During the experiment, acid solution was added to the top of the scroll and then sealed in with dental wax to prevent evaporation. Dental wax was applied to the bottom to prevent leakage and to hold the sample in position. (c) An illustration of the cross-section of a molar. Dentine cuboids were cut from the centre of third molars and placed in the Kapton scrolls with the pulpal side facing up. (d) A representative as-reconstructed slice containing noise in the form of speckling. (e) the filtered reconstructed slice with the segmented tubules highlighted in red.

2.3.2. 3D Data Analysis

The average cross-sectional areas of the tubules were measured using the *Analyze Particles* tool in ImageJ. The maximum size of tubules cross section to be analysed was set to be the size of the largest tubule to prevent bubbles (likely caused by the dissociation of H_2O molecules due to X-ray exposure [32] and CO_2 generated from the reaction between acid and carbonated HAp crystallites) and tubular branching from being included. Tubules at the image borders were excluded from the analysis to avoid underestimated cross-sections. Single pixel and sub-pixel entities were also excluded as these corresponded with small tubules that were too unreliable to include or pixels that were not associated with any tubules. The average tubule diameter was calculated assuming a circular cross-section ($d = \sqrt{4\,A/\pi}$, where A is cross-sectional area). The ITD demineralisation depth was determined from the peak positions of the average size of tubules plots, whereas the PTD demineralisation depth was determined by the 1st order derivative analysis on the average size of tubule plots. Demineralisation rates were then calculated by linear fitting of the demineralisation depth-time plot. From the analysis, no more significant dimensional changes were observed after 180 min so only the analysis results from the first 180 are presented in this paper.

3. Results

3.1. 3D Visualisation

Figure 2 shows the segmented tubules at time points from 15 to 90 min, with an additional rendering at 180 min. Above the demineralised surface, bubbles formed by a combination of the dissociation of H_2O molecules (due to X-ray exposure) and CO_2 generated from the reaction between acid and carbonated HAp and had a similar contrast to the tubules. Immediate observations revealed that the depth of heavily demineralised dentine varied across samples, with Sample#1 demineralised the most and Sample#2 the least. This seemed to correlate with a difference in reaction times as Sample#2 appeared to have stopped demineralising after just 45 mins and Sample#3 after 60 mins whilst Sample#1 was still demineralising at 120 min.

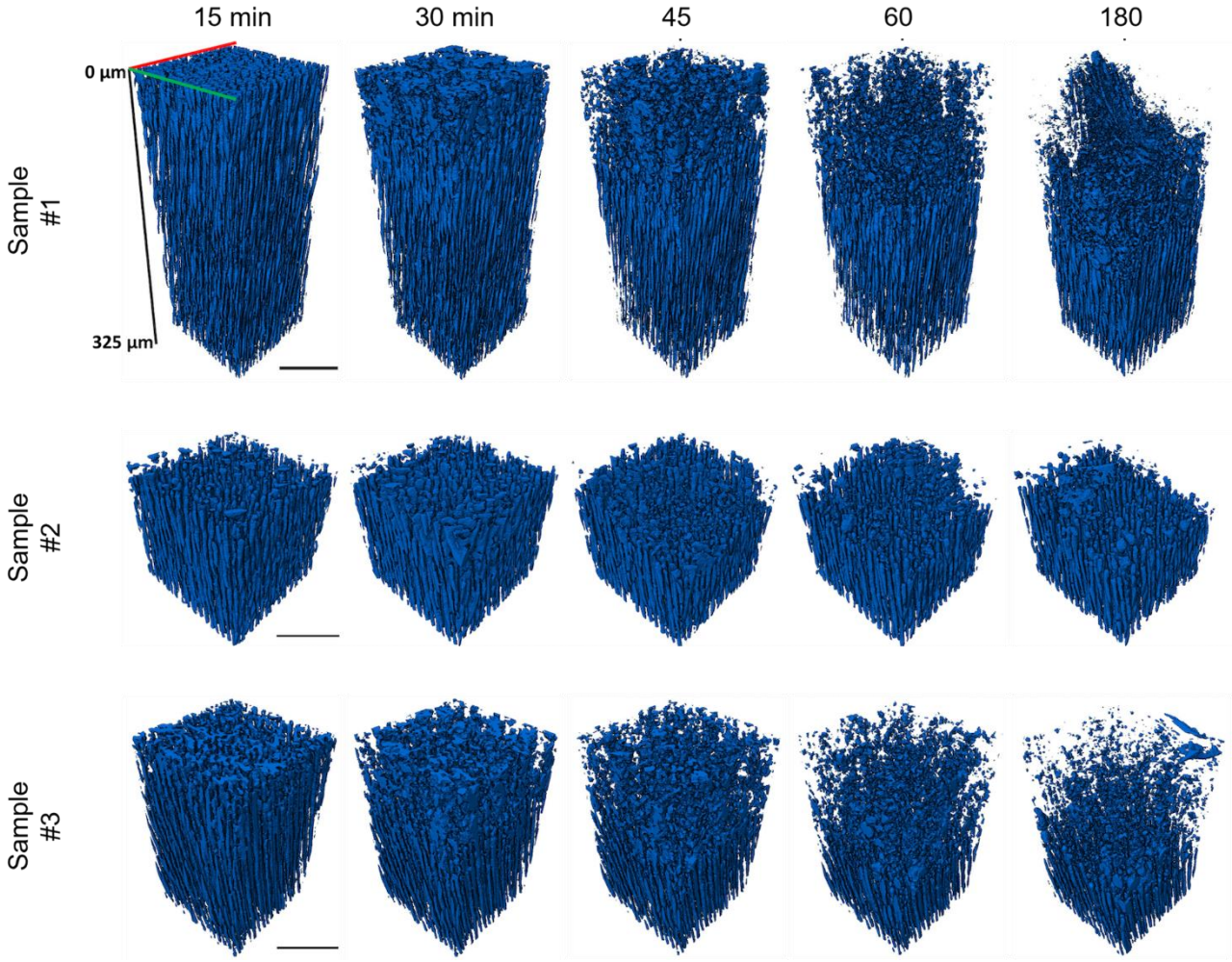

Figure 2 3D structural evolution of tubules over the time. 3D renderings of the inside of the tubules in Sample #1, Sample #2, and Sample #3 at the 15, 30, 45, 60-min timepoints, with an additional rendering of the 180 min timepoint to represent the final state of the samples. The renderings show progressive demineralisation of the dentine, indicated by the reducing height of the tubules (shown as an increasing depth, indicated by the axis shown in Sample #1 at 15 min) and wide tubules near the mineralised surface. The particles above the tubules are the bubbles produced during the acid reaction that had a similar contrast to the tubules and needed to be filtered out during the quantitative analysis. The scale bars are 50 µm for all three samples.

Funnel shaped tubules also formed in all three samples but were more accentuated in Sample#1. Diffusion direction appeared to be predominantly perpendicular to the sample surface, with some parallel diffusion giving rise to the funnel shape of the ITD. This may also have been due to PTD reacting faster to acid, than the ITD, as seen in previous AFM studies [16–20]. Figure 3 shows a series of 2D slices taken from the sample surface to a depth of 50 µm, at 10 µm increments, after 60 min. Close to the top surface, the tubules appeared enlarged where the PTD had been fully demineralised whilst more deeply the tubules appeared smaller with the PTD intact. Significant decreases in the cross-sections were observed at a depth of 20-30 µm in Sample#1, where the PTD began to appear.

In Sample#3, the transition to PTD was less obvious but appeared to occur at a depth of 30-40 µm, whereas there was no obvious transition to PTD in Sample#2. To better observe and quantify these changes, the average diameter of the tubules was measured as a function of depth.

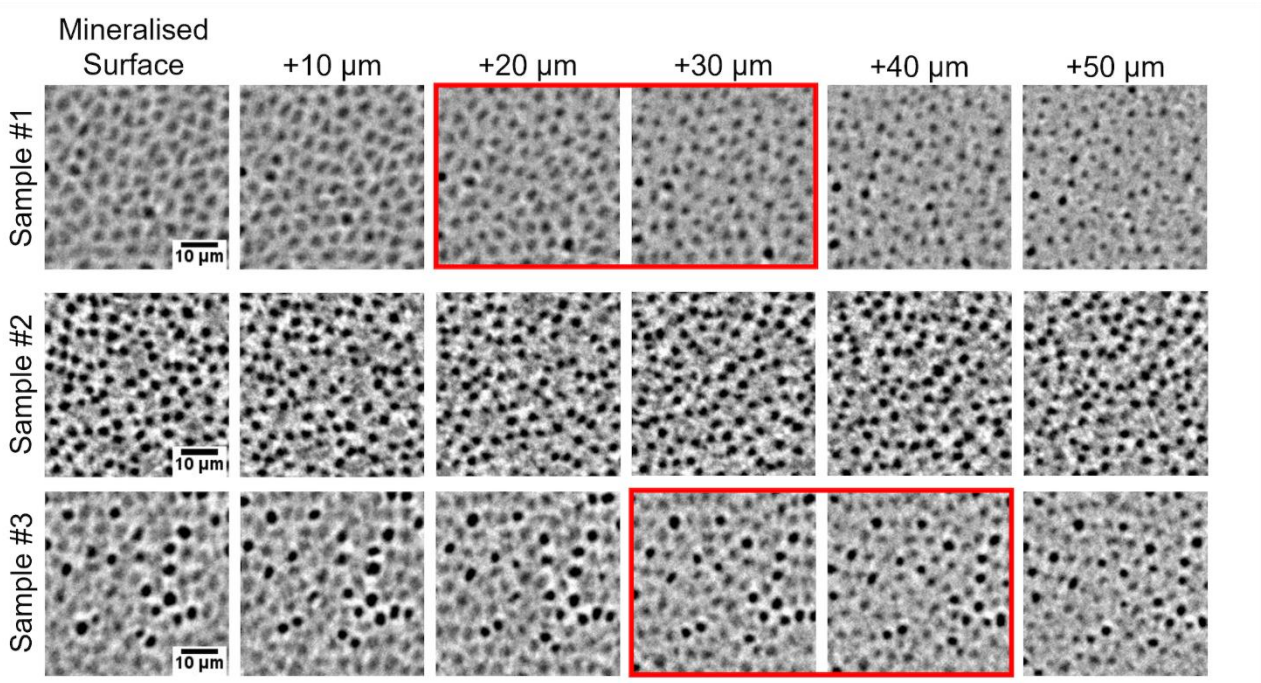

Figure 3 2D structure of tubules with depth. Selected slices, from the 60 min timepoint, starting at the mineralised sample surface and taking 10 µm steps to a depth 50 µm below the mineralised sample surface, showing the funnel shape of the tubules in Sample #1, Sample #2, and Sample #3. Clear transitions from tubules without PTD to tubules with PTD are highlighted in red boxes.

3.2. Tubule Dimensions

Figure 4a-c shows plots of the average tubule diameter with depth, between 15 min and 180 min, where 0 µm depth is the dentine surface (VOI top slice). The plots revealed wider tubules in the superficial layers (narrowing to the typical intact size deeper in the dentine). The baseline tubule diameters were found to be 2.00±0.05 µm, 1.97±0.06 µm, and 1.86±0.06 µm for Sample#1, #2, and #3, respectively, which were within the expected range of 1-3 µm [8]. The depth at which the maximum diameter occurred (indicated by the example arrows in Figure 4a) suggested the demineralisation depth of the ITD surface. In Sample#1 and #3, the peak position could be seen at a greater depth, perhaps due to the continuous demineralisation of the ITD and PTD. The peak position

of Sample#2 gradually shifted by a relatively small amount, stabilising at a depth of ~42 µm after 75 min.

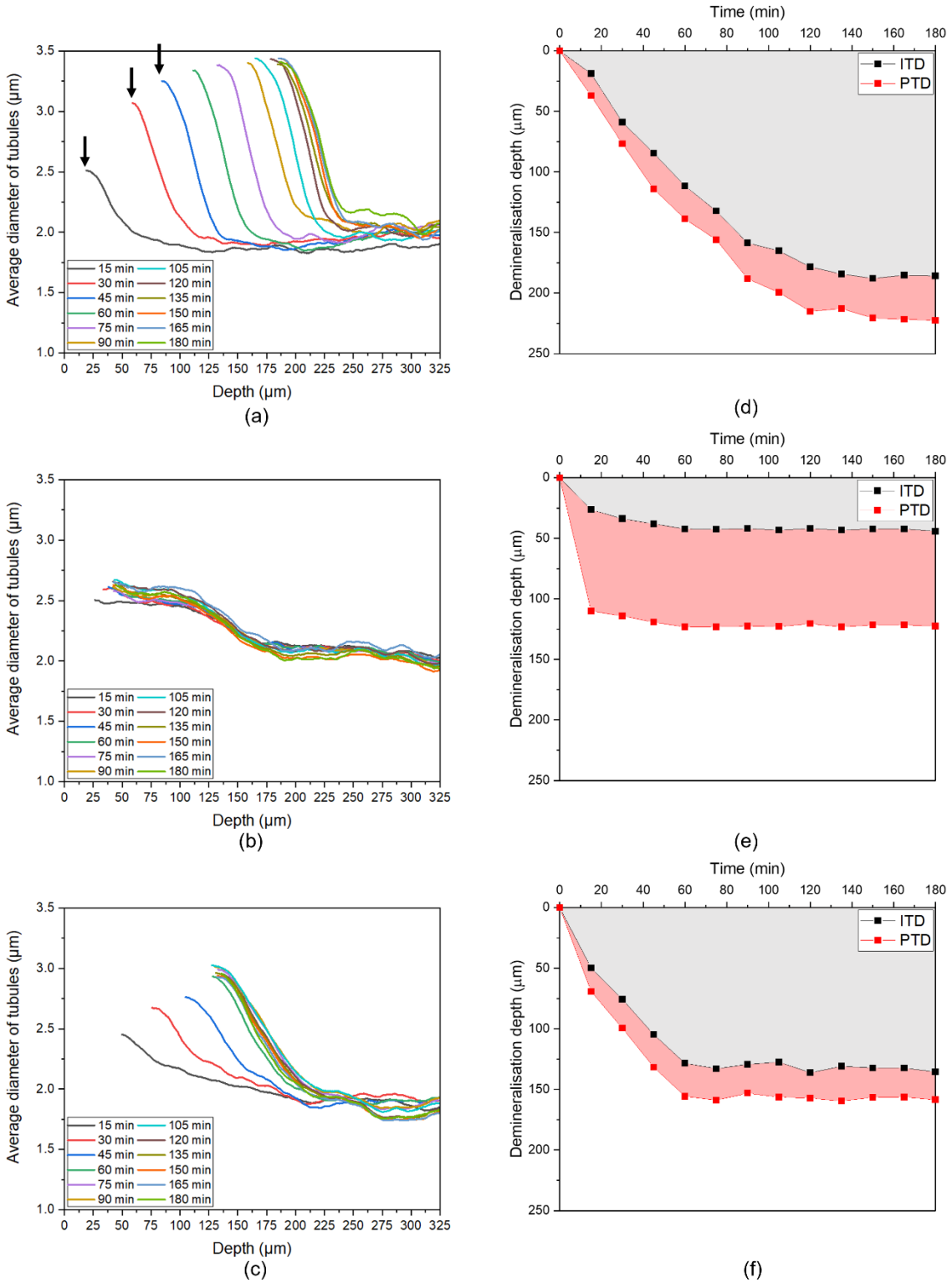

Figure 4 Quantitative analysis of microstructural changes and demineralisation depths with time. Plots of average tubule diameters against depth for each timepoint in (a) Sample #1; (b) Sample #2 and (c) Sample #3. Depth in x-axis corresponds to the height of the VOI from top slice to bottom slice. and demineralisation depth of ITD and PTD against time for (d) Sample #1, (e) Sample #2 and (f) Sample #3. Depth in y-axis corresponds to height of the VOI from top surface to bottom surface.

3.3. Demineralisation Rates

The demineralisation depths of the ITD and PTD were plotted against time in Figure 4d-f, where 0 μm is the top slice of the VOI. Combined observations of the tubule dimensions (Figure 4a-c) and demineralisation depths (Figure 4d-f) suggested that three distinct layers formed during the initial 15 mins of acid demineralisation and remained present throughout the duration of the experiment. The first, superficial, layer was where most of the mineral content (ITD and PTD) had been removed (grey regions in Figure 4d-f). In between the two demineralisation fronts was the second layer (red regions in Figure 4d-f), consisting of intact or partially demineralised ITD with completely demineralised PTD. The third layer at the bottom of the sample, seen below the demineralisation front of PTD (white regions in Figure 4d-f), consisted of intact ITD with intact or partially demineralised PTD. This implied a demineralised collagen matrix was left behind which could not be detected by X-ray microtomography, so SEM was used to investigate the sample surface (next section).

The plots for ITD (black dots), in Samples#1 and #3, the demineralisation depth initially increased linearly with time then plateaued at 120 and 60 min, respectively. A linear fit of the initial linear regions provided ITD demineralisation rates, with R-squared values of 0.99, of 1.80 μm/min and 1.77 μm/min for Sample#1 (15 to 90 min) and Sample#3 (15 to 60 min), respectively. Assuming the ITD demineralisation rate for Sample#2 was initially linear, based on the observations of the other two samples, the rate of ITD demineralisation between the 15 min and 45 min time point would have been approximately 0.50 μm/min. Like the demineralisation profiles for ITD, the demineralisation depth in PTD (red dots) initially increased at a linear rate before reaching a plateau at 120 min and 60 min for Sample#1 and Sample#3, respectively. The difference between the demineralisation rates of ITD and PTD showed that the linear rate of increase was slightly higher in PTD: 1.94 μm/min for both Sample#1 and Sample#3. This difference led to an increasing gap between the demineralisation fronts of ITD and PTD, as highlighted in the red background in Figure 4d-f.

4. Discussion

Imaging 3D dentine structures using SXM, non-destructively made it possible to resolve the ITD and PTD phases. Although SXM has been used to image dentine tubules with submicron resolution, distinctly resolving PTD and ITD has not always been possible due to insufficient phase contrast [21–23] or multiple scans required for high quality tubule reconstruction [24] which prevents capturing fast chemical reactions. In this study, the nominal resolution available was able to resolve most of the tubules in a single scan with some contrast between PTD and ITD. Although PTD is very thin, this method was able to reveal sufficient differences between PTD and the absence of PTD to enable imaging of their features at relatively short time intervals for *in situ* observation. This showed the advantages of SXM for performing time-resolved investigations, monitoring progressive microstructural changes. Future work on developing nanotomography capabilities, with resolutions of tens of nanometres, might better resolve nanostructure and enable more detailed analyses.

It is important to note that the current study is not without limitations. The main limitation being the low sample numbers which did not allow for reliable statistical analysis. This was in part due to an attempt to try 2% v/v lactic acid (pH 2, 100 µL), but the low concentration produced insignificant changes over the duration of the experiment and was therefore not presented, in combination with the general drawback of limited accessibility to synchrotron facilities. There were also discrepancies between the observed dimensional changes in each sample. This was possibly due to acid being applied to the pulpal face of the dentine where new dentine is formed. As such, the structure of this dentine could vary which made interpretation of the data difficult. In addition, there appeared to be some variation in the overall etching times due to the buffering effects of each sample. This could be overcome by using a larger quantity of acid to minimise the effect of the released ions on the pH of the acid solution, possibly increasing the etching time. Furthermore, one of the drawbacks of the current experimental set-up was that the lactic acid solution was not directly agitated throughout the experiment. The result was that the released ions could have produced a so-called “Nernst diffusion

layer" where the acid solution near the mineralised dentine surface became saturated and formed a protective layer, preventing further demineralisation [35]. Agitation of the acid solution would disrupt this layer and enable the demineralisation process to continue [36]. The bubbles produced during the acid reaction could provide some agitation, but direct agitation would have ensured that a Nernst layer did not form. However, due to the nature of synchrotron experiments, manual agitation of the acid solution is not possible and would therefore require a remotely operated device that is safe to use in a synchrotron experimental hutch. Thus, this aspect of the method will require further proof-of-concept work. Despite these limitations, the authors believe that this approach has merit to elucidate the demineralisation process and offers new opportunities for exploring the effects of different acids, pH, and titration on dental demineralisation as well as the potential to study dentine remineralisation for therapeutic purposes.

3D renderings and tomographic slices (Figures 2 and 4) showed widening of the tubules due to preferential demineralisation of the PTD with respect to ITD. A similar phenomenon was reported in *in situ* AFM studies [16–20]. This difference in demineralisation rate was also seen in *ex situ* SEM studies [13,33] where the PTD appeared below the sample surface.

The average demineralisation rate of PTD (1.94 μm/min), calculated here, was similar to values reported in AFM studies, using citric acid (2.13 μm/min) and phosphoric acid (1.29 μm/min) with the same pH values [18]. The main limitation of AFM is the analysis depth (typically ~1.5 μm) which is pertinent here because PTD can quickly dissolved beyond the reach of the AFM tip. This prevents AFM from enabling accurate measurement of ITD demineralisation rates after the first minute, as the ITD demineralisation front continues below the surface of the remaining collagen matrix. The benefit of performing an *in situ* SXM is therefore the ability to continuously monitor the PTD and ITD depths beyond what is achievable by AFM. In this study, PTD and ITD were found to have different linear demineralisation rates (Figure 4), leading to a gradually increasing gap between the depth of ITD and PTD demineralisation fronts. These observations were similar to those of Kinney et al. [25] using *ex situ* SXM to measure mineral density distribution in human dentine during 80 h of interrupted acid

demineralisation who described an intermediate region of uniform mineral density formed between fully demineralised and fully mineralised regions of dentine.

As shown in Figure 4d-f, SXM revealed the formation of three distinct layers, due to the difference in ITD and PTD demineralisation rates. The faster demineralisation rate of PTD created a layer above the intact dentine, which consisted of ITD with fully demineralised PTD. As the demineralisation progressed, the most superficial ITD demineralised to leave a surface layer consisting of collagen. This appeared to be confirmed by SEM and EDX analyses of the sample surfaces, (Supplementary material, Appendix Figure 1), which showed that Sample#3 had tall structures on its surface, with a relatively high *C* content, suggesting that these could be remnants of the collagen matrix layer that had partially remineralised. Although the surfaces of the samples were uneven, which would have compromised the EDX results, it still provided an indication of the elemental changes that occurred in the organic and inorganic phases.

Figure 5 illustrates the observations made in this study. Figure 5a represents intact dentine, with the ITD and PTD. Figure 5b shows the first main route of dentine breakdown where three distinct layers formed and the outer demineralised collagen matrix remained intact. This route was similar to the observations from Sample#3 although the structure of the collagen matrix appeared disturbed possibly by the gas bubbles produced during the experiment. Figure 5c shows a second route which started with the formation of the three layers except that the demineralised collagen matrix was stripped from the sample surface, as seen in Sample#2. Sample#1 appeared somewhere between the two, with the collagen mostly stripped away with remnants collapsing onto the sample surface and remineralisation. The illustrations in Figure 5 may seem similar to those in [34], which were based on observations made using AFM and, as previously mentioned, are only reliable for the initial stages of demineralisation in the top ~2 μm where the mineralised dentine was still accessible by the probe. With SXM, it is possible to continue monitoring the mineralised phase at much greater depths beyond the sample surface and the initial stages of demineralisation.

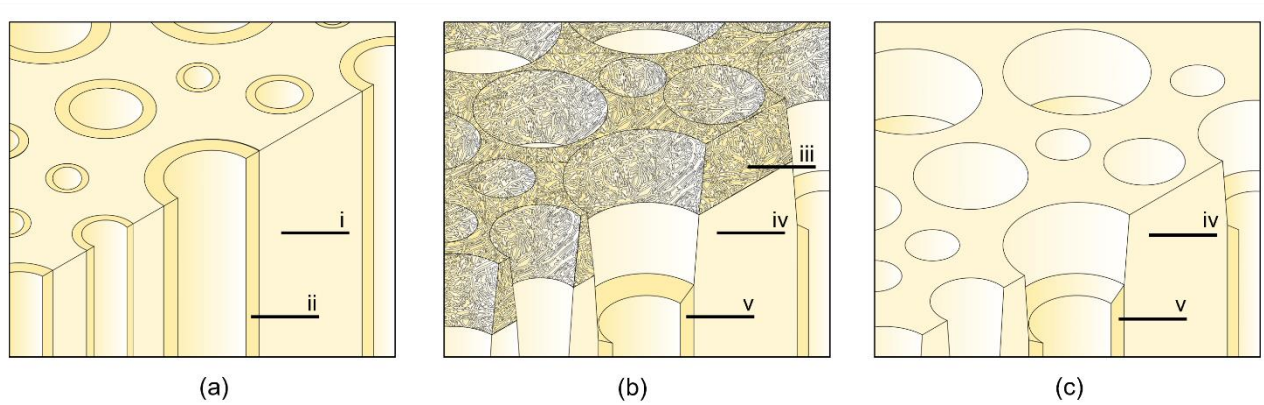

Figure 5 A demineralisation process of dentine. (a) shows the state of dentine, before acid exposure, with the ITD (i) and PTD (ii) intact. During acid demineralisation, the samples in this study appeared to undergo two main routes of breakdown. (b) shows the first route where dentine forms three distinct layers: a layer of completely demineralised collagen matrix (iii), a layer of intact/partially demineralised ITD and fully demineralised PTD (iv), and a layer of intact ITD with intact/partially demineralised PTD (v). In (c), the three layers are also formed except the upper layer of demineralised collagen is stripped from the sample surface.

5. Conclusion

High-speed SXM has been shown to be suitable method for measuring the dissolution rates of ITD and PTD whilst providing the ability to study relatively large volumes of dentine. Although AFM is more convenient, the ability to monitor the progressive demineralisation in dentine to a greater depth is more worthwhile.

In summary, observations made with this technique, such as those made in the present study, could lead to the establishment of reliable numerical models of dentine demineralisation and the subsequent effects on the mechanical properties of dentine [35].

References

[1] Taji S, Seow WK. A literature review of dental erosion in children. Aust Dent J 2010;55:358–67. https://doi.org/10.1111/j.1834-7819.2010.01255.x.

[2] Scheutzel P. Etiology of dental erosion--intrinsic factors. Eur J Oral Sci 1996;104:178–90. https://doi.org/10.1111/j.1600-0722.1996.tb00066.x.

[3] Zero DT. Etiology of dental erosion-extrinsic factors. Eur J Oral Sci 1996;104:162–77.

https://doi.org/10.1111/j.1600-0722.1996.tb00065.x.

[4] Shellis RP. The dental erosion process. Dental Erosion and Its Clinical Management, 2015, p. 13–33. https://doi.org/10.1007/978-3-319-13993-7_2.

[5] Featherstone JD, Lussi A. Understanding the chemistry of dental erosion. Monogr Oral Sci 2006;20:66–76. https://doi.org/10.1159/000093351.

[6] Skucha-Nowak M, Gibas M, Tanasiewicz M, Twardawa H, Szklarski T. Natural and controlled demineralization for study purposes in minimally invasive dentistry. Adv Clin Exp Med 2015;24:891–8. https://doi.org/10.17219/acem/28903.

[7] Hara AT, Zero DT. The Potential of Saliva in Protecting against Dental Erosion. Monogr Oral Sci 2014;25:197–205. https://doi.org/10.1159/000360372.

[8] Linde A, Goldberg M. Dentinogenesis. Crit Rev Oral Biol Med 1994;4:679–728. https://doi.org/10.1177/10454411930040050301.

[9] Goldberg M, Kulkarni AB, Young M, Boskey A. Dentin: Structure, composition and mineralization. Front Biosci - Elit 2011;3 E:711–35. https://doi.org/10.2741/e281.

[10] Sui T, Dluhoš J, Li T, Zeng K, Cernescu A, Landini G, et al. Structure-function correlative microscopy of peritubular and intertubular dentine. Materials (Basel) 2018;11. https://doi.org/10.3390/ma11091493.

[11] Meurman JH, Drysdale T, Frank RM. Experimental erosion of dentin. Eur J Oral Sci 1991;99:457–62. https://doi.org/10.1111/j.1600-0722.1991.tb01054.x.

[12] Hannas AR, Pereira JC, Granjeiro JM, Tjäderhane L. The role of matrix metalloproteinases in the oral environment. Acta Odontol Scand 2007;65:1–13. https://doi.org/10.1080/00016350600963640.

[13] Xu Z, Neoh KG, Kishen A. Monitoring acid-demineralization of human dentine by electrochemical impedance spectroscopy (EIS). J Dent 2008;36:1005–12. https://doi.org/10.1016/j.jdent.2008.08.007.

[14] Chien YC, Burwell AK, Saeki K, Fernandez-Martinez A, Pugach MK, Nonomura G, et al.

Distinct decalcification process of dentin by different cariogenic organic acids: Kinetics, ultrastructure and mechanical properties. Arch Oral Biol 2016;63:93–105. https://doi.org/10.1016/j.archoralbio.2015.10.001.

[15] Kinney JH, Balooch M, Marshall SJ, Marshall GW, Weihs TP. Atomic force microscope measurements of the hardness and elasticity of peritubular and intertubular human dentin. J Biomech Eng 1996;118:133–5. https://doi.org/10.1115/1.2795939.

[16] Marshall GW, Balooch M, Tench RJ, Kinney JH, Marshall SJ. Atomic force microscopy of acid effects on dentin. Dent Mater 1993;9:265–8. https://doi.org/10.1016/0109-5641(93)90072-X.

[17] Marshall GW, Balooch M, Kinney JH, Marshall SJ. Atomic force microscopy of conditioning agents on dentin. J Biomed Mater Res 1995;29:1381–7. https://doi.org/10.1002/jbm.820291109.

[18] Marshall GW, Inai N, Wu-Magidi IC, Balooch M, Kinney JH, Tagami J, et al. Dentin demineralization: effects of dentin depth, pH and different acids. Dent Mater 1997;13:338–43. https://doi.org/10.1016/s0109-5641(97)80104-2.

[19] Marshall GW, Wu-Magidi IC, Watanabe LG, Inai N, Balooch M, Kinney JH, et al. Effect of citric acid concentration on dentin demineralization, dehydration, and rehydration: Atomic force microscopy study. J Biomed Mater Res 1998;42:500–7. https://doi.org/10.1002/(SICI)1097-4636(19981215)42:4<500::AID-JBM4>3.0.CO;2-L.

[20] Marshall GW, Marshall SJ, Balooch M, Kinney JH. Evaluating demineralization and mechanical properties of human dentin with AFM. Methods Mol Biol 2004;242:141–59. https://doi.org/10.1385/1-59259-647-9:141.

[21] Deyhle H, Weitkamp T, Lang S, Schulz G, Rack A, Zanette I, et al. Comparison of propagation-based phase-contrast tomography approaches for the evaluation of dentin microstructure. Dev. X-Ray Tomogr. VIII, 2012. https://doi.org/10.1117/12.929951.

[22] Deyhle H, Bunk O, Buser S, Krastl G, Zitzmann NU, Ilgenstein B, et al. Bio-inspired dental

fillings. Biomimetics and Bioinspiration, vol. 7401, 2009, p. 74010E. https://doi.org/10.1117/12.827437.

[23] Zaslansky P, Zabler S, Fratzl P. 3D variations in human crown dentin tubule orientation: A phase-contrast microtomography study. Dent Mater 2010;26. https://doi.org/10.1016/j.dental.2009.09.007.

[24] Zabler S, Cloetens P, Zaslansky P. Fresnel-propagated submicrometer x-ray imaging of water-immersed tooth dentin. Opt Lett 2007;32:2987. https://doi.org/10.1364/ol.32.002987.

[25] Kinney JH, Balooch M, Haupt DL, Marshall SJ, Marshall GW. Mineral Distribution and Dimensional Changes in Human Dentin during Demineralization. J Dent Res 1995;74:1179–84. https://doi.org/10.1177/00220345950740050601.

[26] Harper RA, Shelton RM, James JD, Salvati E, Besnard C, Korsunsky AM, et al. Acid-induced demineralisation of human enamel as a function of time and pH observed using X-ray and polarised light imaging. Acta Biomater 2020;120:240–8. https://doi.org/10.1016/j.actbio.2020.04.045.

[27] Basham M, Filik J, Wharmby MT, Chang PCY, El Kassaby B, Gerring M, et al. Data Analysis WorkbeNch(DAWN). J Synchrotron Radiat 2015;22:853–8. https://doi.org/10.1107/S160057751500228.

[28] Titarenko V, Titarenko S, Withers PJ, De Carlo F, Xiao X. Improved tomographic reconstructions using adaptive time-dependent intensity normalization. J Synchrotron Radiat 2010;17:689–99. https://doi.org/10.1107/S0909049510024908.

[29] Schindelin J, Arganda-Carreras I, Frise E, Kaynig V, Longair M, Pietzsch T, et al. Fiji: An open-source platform for biological-image analysis. Nat Methods 2012;9:676–82. https://doi.org/10.1038/nmeth.2019.

[30] Schneider CA, Rasband WS, Eliceiri KW. NIH Image to ImageJ: 25 years of image analysis. Nat Methods 2012;9:671–5. https://doi.org/10.1038/nmeth.2089.

[31] Otsu N. Threshold Selection Method From Gray-Level Histograms. IEEE Trans Syst Man

Cybern 1979;SMC-9:62–6. https://doi.org/10.1109/tsmc.1979.4310076.

[32] Mao WL, Mao HK, Meng Y, Eng PJ, Hu MY, Chow P, et al. X-ray-induced dissociation of H2O and formation of an O 2-H2 alloy at high pressure. Science (80-) 2006;314:636–8. https://doi.org/10.1126/science.1132884.

[33] Lussi A, Schlueter N, Rakhmatullina E, Ganss C. Dental erosion - An overview with emphasis on chemical and histopathological aspects. Caries Res 2011;45:2–12. https://doi.org/10.1159/000325915.

[34] Sakaguchi RL, Ferracane JL, Powers JM. Craig's restorative dental materials. 2018. https://doi.org/10.1016/C2015-0-01767-1.

[35] Hu J, Sui T. Insights into the reinforcement role of peritubular dentine subjected to acid dissolution. J Mech Behav Biomed Mater 2020;103:103614. https://doi.org/10.1016/j.jmbbm.2019.103614.

Acknowledgements

The authors give thanks to Dr Jonathan James from the University of Birmingham, for his help in preparing samples used in this work. The authors would also like to thank Dr Shashidhara Marathe, and Dr Kazimir Wanelik, from the I13 beamlines at Diamond Light Source (DLS), for their support and assistance with data acquisition, reduction and analysis. DLS is also acknowledged for providing access to the I13-2 facilities under the allocation MT20155. The EPSRC project (EP/S022813/1) "Understanding and enhancing the mechanical performance of bioinspired zirconia-based dental materials" is acknowledged for the funding support.

N. Leung contributed to the design, data acquisition, analysis, and interpretation, drafted and critically revised the manuscript. R.A. Harper contributed to data acquisition and interpretation, critically revised the manuscript. B. Zhu contributed to data acquisition, drafted and critically revised the manuscript. G. Landini, R.M. Shelton contributed to conception, data interpretation, and critically revised the manuscript. T. Sui contributed to conception, design, data acquisition, analysis, and

interpretation, drafted and critically revised the manuscript. All authors gave their final approval and agree to be accountable for all aspects of the work.

The authors declare no potential conflicts of interest with respect to the authorship and/or publication of this article.

Supplementary Material

Scanning Electron Microscopy (SEM) and Energy Dispersive X-ray Analysis (EDX)

Samples #1 to #3 were coated with a 4-6 nm Au layer using an Emitech K575X sputter coater (Quorum Technologies Ltd, UK) and then visualised using a field emission FIB-SEM (FERA3, TESCAN, Brno, Czechia), in back-scattered (BSE) mode, with an accelerating voltage of 5 kV. EDX analysis was performed in a JEOL JSM-7100F SEM (JEOL (UK) Ltd, UK) with an UltraDry EDX detector (Thermo Scientific, USA) and an accelerating voltage of 15 kV. *Ca*, *P*, *O*, and *C* were selected for quantitative elemental analysis and a region near the centre of the sample surface was analysed initially at a magnification of 700× before using 2000× to analyse specific features within this region.

To determine the status of the collagen matrix, SEM Backscattered-Electron (BSE) micrographs (shown in Supplementary Figure 1) of the top surfaces of the as-demineralised samples were collected. On immediate inspection, each sample appeared to have different responses to acid demineralisation. In Sample #1 (Supplementary Figure 1 a), the tubules could be seen to have very large openings, as previously seen in the 3D reconstructions (Figure 2). There also appeared to be an abundance of material deposits in addition to some crystal formation. A higher magnified micrograph of the centre region (Supplementary Figure 1 d) shows the enlarged tubules and material deposits in more detail. Conversely, Sample #2 (Supplementary Figure 1 b) had a very uneven surface with only a few small deposits visible on the surface. Note that the scrape on the surface was accidental damage caused during sample removal from the Kapton cylinder. The surface of Sample #3 (Supplementary Figure 1 c) showed tall structures which displayed signs of having a pre-existing tubular structure,

indicated by what appear to be tubules within some of the structures. Some examples of these surviving tubules can be seen on the right of Supplementary Figure 1 f.

EDX analyses were performed on the material deposits, seen on Sample #1 (Supplementary Figure 1 d), and the tall structures, seen on Sample #3 (Supplementary Figure 1 f), to help reveal the demineralisation process that had occurred in each sample. EDX maps were captured to quantify the distribution of *Ca* and *P*, relating to HAp crystallites, and *C*, relating to organic collagen. In Sample #1, comparison of the elemental distributions in the material deposits (centre of Supplementary Figure 1 g) and the exposed tubules (left and top-right of Supplementary Figure 1 g) showed a comparable *C* content of 7.21 at%, 6.92 at%, and 7.03 at%, respectively, suggesting that the quantity of organic phase remained unchanged. Comparing the *Ca*/*P* ratios in these regions, which provides an indication of the crystallite species present, showed that the material deposits had a slightly higher *Ca/P* ratio (2.07 compared with 1.91 and 1.65 in the left and top-right exposed tubule regions, respectively), suggesting that these structures may correspond to a re-precipitation of calcium phosphate. Furthermore, shifts towards a higher *Ca/P* ratio on the exposed tubules, from a ratio of 1.67 for HAp, indicated a preferential loss of phosphate compared with calcium during demineralisation. In Sample #3, the topography of the sample surface meant that deeper regions were obscured from elemental detection, particularly the areas that appeared as voids in Supplementary Figure 1 f. These regions therefore appeared as greyscale in Supplementary Figure 1 i. Due to the inability to analyse the tubules in the deeper regions of Supplementary Figure 1 f, elemental analysis was instead performed on the regions of exposed tubules in the bottom and mid-left areas of Supplementary Figure 1 c. Elemental analysis showed that the tall structures had a *C* content that was twice that of the exposed tubules of that sample, which suggested that the collagen matrix had not remineralised. Calculating the *Ca*/*P* ratios in these structures and the exposed tubule regions gave a ratio of 2.03 in the tall structures and ratios of 1.97 and 1.75 in the bottom and mid-left exposed tubule regions in Supplementary Figure 1 c, respectively. These ratios again indicated that there had been preferential phosphate loss during demineralisation. In Sample #2, EDX was performed on the tubules shown in

Supplementary Figure 1 e. The ratio of *Ca*/*P* in these tubules was 1.75 which is comparable to the ratios seen in the exposed tubule regions in Samples #1 and #3.

As previously mentioned in section 3.3, the SXM showed that three distinct layers formed during exposure to acid and these three layers appeared to be present in the SEM images. From SEM and EDX observations, there appeared to be three different demineralisation mechanisms taking place. In Supplementary Figure 1 a, the wide tubules were the result of the PTD being completely demineralised, as well as some of the ITD, which would indicate that the ITD here was part of the second distinct layer. This suggested that the deposits on the sample surface were debris from where the fully demineralised collagen had been partially stripped and the remaining collagen has then collapsed onto the sample surface and remineralised. In Supplementary Figure 1 b, the uneven surface showed clear signs of demineralisation. However, there was a distinct lack of surface deposits, like those seen in Supplementary Figure 1 a, which indicated that all of the demineralised collagen matrix was removed in Sample #2. In Supplementary Figure 1 c, the tall structures, with a relatively high *C* content, appeared to be the remnants of the fully demineralised collagen matrix layer (now partially remineralised). The malformity was likely due to the bubbles, generated during the experiment, displacing the collagen fibres from the original tubule like structure.

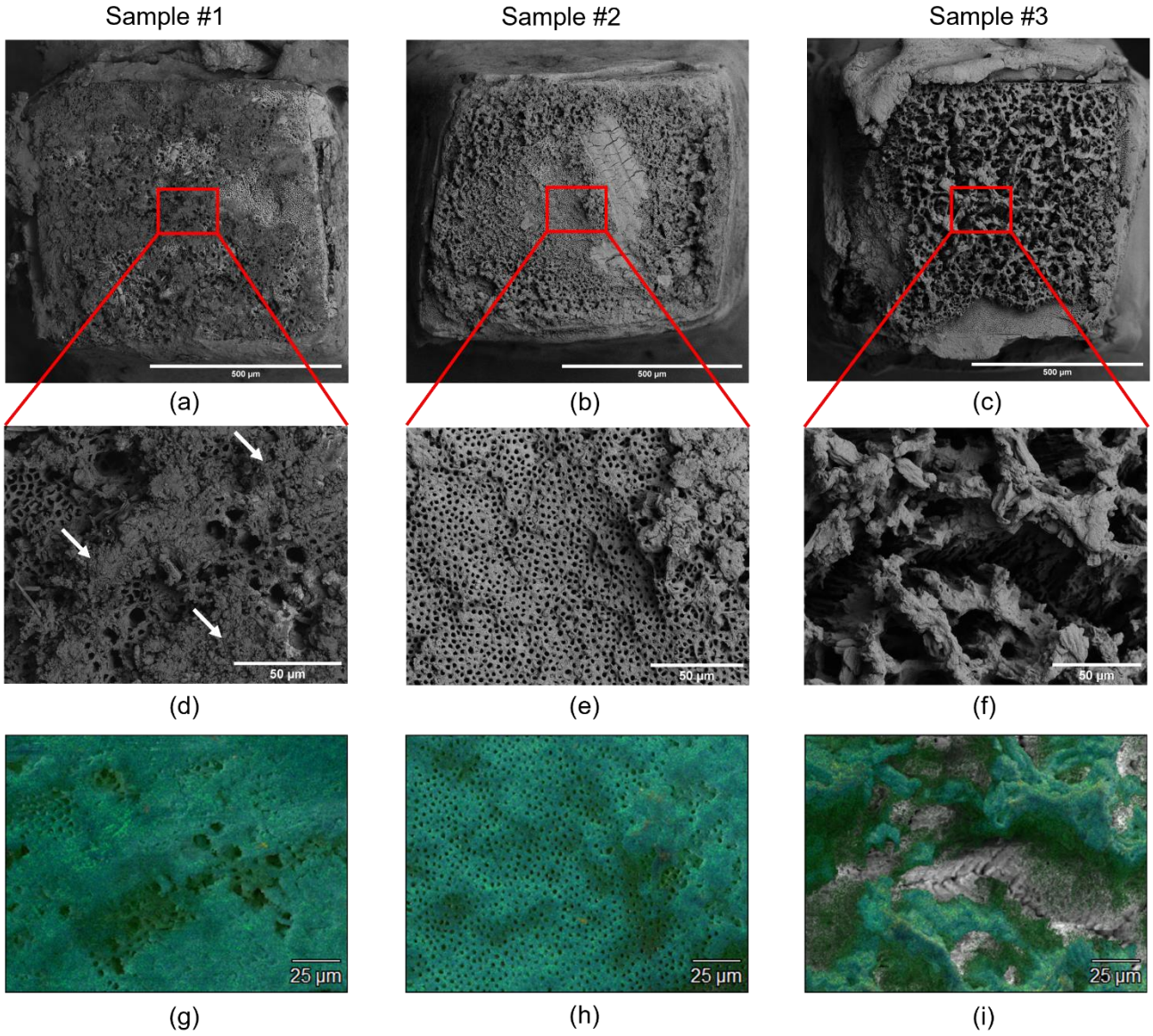

Supplementary Figure 1 Microstructure and chemical composition of as demineralised sample surfaces. SEM back-scattered electron micrographs of (a) Sample #1; (b) Sample #2 and (c) Sample #3. SEM backscattered electron micrographs of ROIs in (d-f) in Samples 1-3. (g-i) combined EDX maps of *Ca*, *P*, *O*, and *C* in the ROIs of each sample. The greyscale regions in (i) are due to a lack of detection caused by the topography of the sample surface.